Journal of ELECTRONIC MATERIALS, Vol. 42, No. 2, 2013
DOI: 10.1007/s11664-012-2227-y
© 2012 TMS

Creep and Mechanical Properties of Cu_6Sn_5 and $(Cu,Ni)_6Sn_5$ at Elevated Temperatures

DEKUI MU,[1,2,3] HAN HUANG,[2] STUART D. MCDONALD,[1] and KAZUHIRO NOGITA[1]

1.—Nihon Superior Centre for the Manufacture of Electronic Materials, School of Mechanical & Mining Engineering, The University of Queensland, Brisbane, QLD 4072, Australia. 2.—School of Mechanical & Mining Engineering, The University of Queensland, Brisbane, QLD 4072, Australia. 3.—e-mail: dekui.mu@uqconnect.edu.au

Cu_6Sn_5 is the most common and important intermetallic compound (IMC) formed between Sn-based solders and Cu substrates during soldering. The Cu_6Sn_5 IMC exhibits significantly different thermomechanical properties from the solder alloys and the substrate. The progress of high-density three-dimensional (3D) electrical packaging technologies has led to increased operating temperatures, and interfacial Cu_6Sn_5 accounts for a larger volume fraction of the fine-pitch solder joints in these packages. Knowledge of creep and the mechanical behavior of Cu_6Sn_5 at elevated temperatures is therefore essential to understanding the deformation of a lead-free solder joint in service. In this work, the effects of temperature and Ni solubility on creep and mechanical properties of Cu_6Sn_5 were investigated using energy-dispersive x-ray spectroscopy and nanoindentation. The reduced modulus and hardness of Cu_6Sn_5 were found to decrease as temperature increased from 25°C to 150°C. The addition of Ni increased the reduced modulus and hardness of Cu_6Sn_5 and had different effects on the creep of Cu_6Sn_5 at room and elevated temperatures.

Key words: Intermetallic compounds, nanoindentation, mechanical properties, lead-free solder

INTRODUCTION

The continuous performance demands and progress of three-dimensional (3D) electrical packaging technologies has led to increased Joule heating and accompanying operating temperature[1] of lead-free solder joints. Moreover, the volume fraction of IMCs in a typical lead-free solder joint has increased, and interfacial IMCs account for a larger fraction of the joint microstructure because of the minimization of solder joints in 3D integrated circuits (ICs).[2] The diameter of a solder joint in a traditional ball grid array (BGA) is typically around 100 μm, although this is expected to reduce to approximately 1 μm in 3D ICs.[3] In this scenario, the solder alloys can conceivably be completely consumed and a solder joint may consist of a few grains of intermetallic compounds (IMCs).[2,3] As a result, the deformation behavior of a lead-free solder joint is determined by the mechanical properties of the IMCs rather than the solder alloys.[4]

Cu_6Sn_5 is an important intermetallic compound (IMC) because it is commonly formed during interface reactions between most Sn-based solders and Cu substrates.[5] For solder joints in 3D ICs, Cu_6Sn_5 is expected to be the dominant phase in the joint microstructure even after the aging processes. Thus, the mechanical properties of Cu_6Sn_5 play a determinant role in the overall deformation of a solder joint in 3D ICs. The mechanical properties of Cu_6Sn_5 have been studied both experimentally and theoretically during the last decade.[6–9] Nanoindentation has been proven as a suitable method to investigate the mechanical properties of IMCs formed in diffusion samples,[6] at the solder–substrate interface,[7,9] and in bulk IMCs formed by solidification and diffusion.[10] These previous experimental results are in good agreement with

(Received April 20, 2012; accepted August 6, 2012; published online September 11, 2012)

Table I. Sample chemical compositions of Cu_6Sn_5 and $(Cu,Ni)_6Sn_5$

Nominal Stoichiometry	Analyzed Nickel Content (wt.%)
Cu_6Sn_5	0.0
$Cu_{5.5}Ni_{0.5}Sn_5$	4.0 ± 0.9
$Cu_5Ni_1Sn_5$	6.3 ± 0.7
$Cu_{4.5}Ni_{1.5}Sn_5$	10.1 ± .08
$Cu_4Ni_2Sn_5$	14.6 ± 0.5

theoretical computations.[11] Using the electron backscattered diffraction (EBSD) technique, directionally solidified hexagonal Cu_6Sn_5 was found to have anisotropic mechanical properties,[12] and it has been suggested that this anisotropy in mechanical properties may affect crack formation due to the altered growth textures in Cu_6Sn_5 and $(Cu,Ni)_6Sn_5$ layers.[13,14] Recently, Sun et al.[15] investigated the creep of several IMCs formed during lead-free soldering at room temperature. However, the creep and mechanical properties of Cu_6Sn_5 at elevated temperatures are not available in literature.

Ni is an important alloying element in Sn-Cu lead-free solders. The addition of Ni has been associated with such benefits as superior solidification microstructures, increased volume fraction of the eutectic phase, and lower propensity for interfacial IMCs to crack during service.[16,17] Ni is also actively involved in the interface reaction and has a remarkable influence on the formation and properties of Cu_6Sn_5.[18] It has been reported that Ni can reduce the enthalpy of Cu_6Sn_5, so the formed $(Cu,Ni)_6Sn_5$ has a more negative heat of formation.[19,20] Nogita et al.[21,22] found that Ni stabilizes hexagonal Cu_6Sn_5, inhibiting the hexagonal to monoclinic transformation that, at equilibrium, occurs at 186°C. Ni can also reduce the thermal expansion coefficient of Cu_6Sn_5[23,24] and increase the elastic modulus and hardness of Cu_6Sn_5.[7,9] At room temperature, linear relationships between Ni concentration and the mechanical properties of Cu_6Sn_5 were reported in our previous study for both elastic modulus and hardness.[10] However, the effect of Ni solubility on the creep and mechanical properties of Cu_6Sn_5 at elevated temperatures still remains unknown.

In this research, the creep and mechanical properties of Cu_6Sn_5 and $(Cu,Ni)_6Sn_5$ from 25°C to 150°C were investigated using nanoindentation. Energy-dispersive x-ray spectroscopy (EDS) analysis was used to confirm the chemical composition of each sample, prior to and after nanoindentation at elevated temperatures.

EXPERIMENTAL PROCEDURES

Samples of $Cu_{6-x}Ni_xSn_5$ (x = 0, 0.5, 1, 1.5, 2) IMCs were prepared by direct casting; the chemical composition of each sample is summarized in Table I. Detailed sample preparation was described in our previous research.[16,17] Microstructural observations and elemental analyses were conducted using a JEOL 6460 (JEOL, Tokyo, Japan) scanning electron microscope (SEM) with EDS capabilities. The nickel contents in the $(Cu,Ni)_6Sn_5$ alloys shown in Table I were measured by averaging the multiple measurements taken on the samples. For the nominal compositions of Ni associated with thermal expansions and lattice parameters of $Cu_{6-x}Ni_xSn_5$ (x = 0, 0.5, 1, 1.5, 2) IMCs measured by synchrotron diffraction, please refer to our previous study.[23] Mechanical properties (reduced modulus and hardness) of the IMCs were measured using a Hysitron Triboindenter (Hysitron, MN, USA).[25] A Berkovich diamond indenter with tip radius of 100 nm was used. Each nanoindentation test consisted of three stages: loading, dwell at target load, and unloading. The indentation load of 2000 μN was applied at loading rate of 200 μN/s, and the dwell times at peak load were 1 s and 60 s for mechanical properties and creep measurements, respectively. The unloading rate was -166.67 μN/s. A heating stage with maximum temperature of 400°C was used to control the temperatures for nanoindentation, which was monitored by a T-type thermocouple directly mounted on the surface of the sample. The tolerance of temperature variation was less than 5°C. During heating/cooling, the indentation tip was disengaged and located 1 μm away from the top surfaces of samples. Once the required temperature was reached, the output current of the heating stage was held for at least 1 h to establish thermal equilibrium between the sample and the indention tip. The mechanical properties of $Cu_{6-x}Ni_xSn_5$ (x = 0, 0.5, 1, 1.5, 2) were measured at 25°C, 75°C, 100°C, 125°C, and 150°C, and the creep of Cu_6Sn_5 and $Cu_{5.5}Ni_{0.5}Sn_5$ were characterized at 25°C, 125°C, and 150°C. Reduced modulus, hardness, and creep properties were obtained by averaging multiple tests.

Load-control depth-sensitive nanoindentation was used to measure the mechanical properties of the IMCs. From the load–displacement curve obtained in a nanoindentation test, the mechanical properties of a material were extracted. As a depth-sensitive method, the first step of a nanoindentation test was to determine the relationship between indentation displacement h and contact area A defined as

$$A = C_0 \cdot h^2 + C_1 \cdot h + C_2 \cdot \sqrt{h} + C_3 \cdot \sqrt[4]{h} + C_4 \cdot \sqrt[8]{h} + C_5 \cdot \sqrt[16]{h}, \quad (1)$$

where $C_0 = 24.5$, $C_1 = 2.59 \times 10^4$, $C_2 = -2.59 \times 10^6$, $C_3 = 2.90 \times 10^7$, $C_4 = -7.43 \times 10^7$, $C_5 = 4.78 \times 10^7$. The detailed methods used to determine the reduced modulus E_r and hardness H can be found in previous studies.[7,9] The nanoindentation test was also used to examine the creep behavior of a material from the displacement curve during dwell time at the peak load.[26] In this study, a constant peak

load test was conducted to measure the creep of Cu_6Sn_5 and $Cu_{5.5}Ni_{0.5}Sn_5$ at 25°C, 125°C, and 150°C. From the indentation creep displacement curve $h(t)$ during dwell time, the creep strain rate and stress were calculated using the following equations, respectively:

$$\dot{\varepsilon} = \frac{1}{h} \cdot \frac{\mathrm{dh}}{\mathrm{d}t}, \tag{2}$$

$$\sigma = \frac{P_{\max}}{A}, \tag{3}$$

where $h(t)$ is the indentation creep displacement during dwell time and A is the contact area. It is worth noting that the contact area A in Eq. 3 is a function of the creep displacement $h(t)$ and hence time dependent. The creep strain rate $\dot{\varepsilon}$ was thus calculated by fitting the displacement curve $h(t)$. The creep strain rate $\dot{\varepsilon}$, creep strain stress σ, and creep stress exponent n can then be determined through the following relationships:[27]

$$\dot{\varepsilon} = k \cdot \sigma^n, \tag{4}$$

$$\log\left(\frac{1}{h} \cdot \frac{\mathrm{dh}}{\mathrm{d}t}\right) = \log k + n \cdot \log\left(\frac{P_{\max}}{A}\right), \tag{5}$$

where k is a constant. The creep stress exponent n was determined from the log–log plot. By log–log plotting of the steady creep strain rates against the reciprocal of absolute temperature at constant indentation stress $P_{\max}/A$, the creep activation energy was calculated as:

$$Q = -K \cdot \left[\frac{\partial \log \dot{\varepsilon}}{\partial (1/T)}\right]_{P_{\max}/A}, \tag{6}$$

where K is Boltzmann's constant.

RESULTS AND DISCUSSION

Figure 1 shows the representative load–displacement behavior during indentation of Cu_6Sn_5 at 25°C and 150°C, and these data indicate that Cu_6Sn_5 has more elastic recovery than solder alloys.[27–29] As the temperature increased, the maximum indentation depth increased around one-third from 120 nm to 160 nm. This indicates that Cu_6Sn_5 was softened at elevated temperatures.

Figure 2a shows the reduced modulus of $Cu_{6-x}Ni_xSn_5$ (x = 0, 0.5, 1, 1.5, 2) from 25°C to 150°C. At 150°C, the reduced modulus of Cu_6Sn_5 is 54.27 ± 4.54 GPa, which is less than half of the value of 124.26 ± 7.93 GPa at 25°C. The decrease in reduced modulus at elevated temperatures is because the elastic modulus represents the interatomic force[30] and is inversely proportional to a power N of the distance X_0 between adjacent atoms,

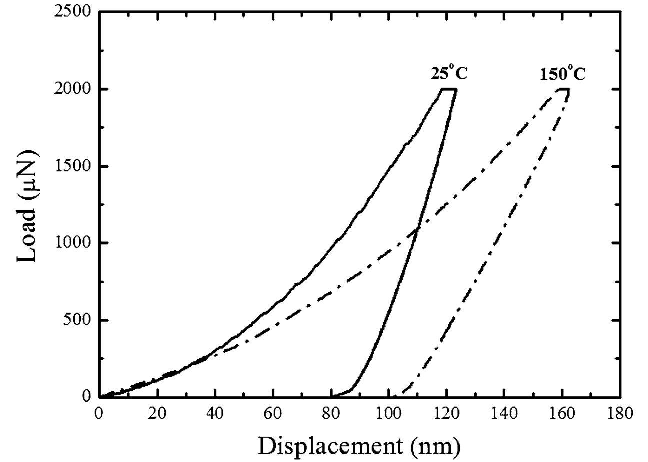

Fig. 1. Representative displacement–load curve at 25°C and 150°C for Cu_6Sn_5.

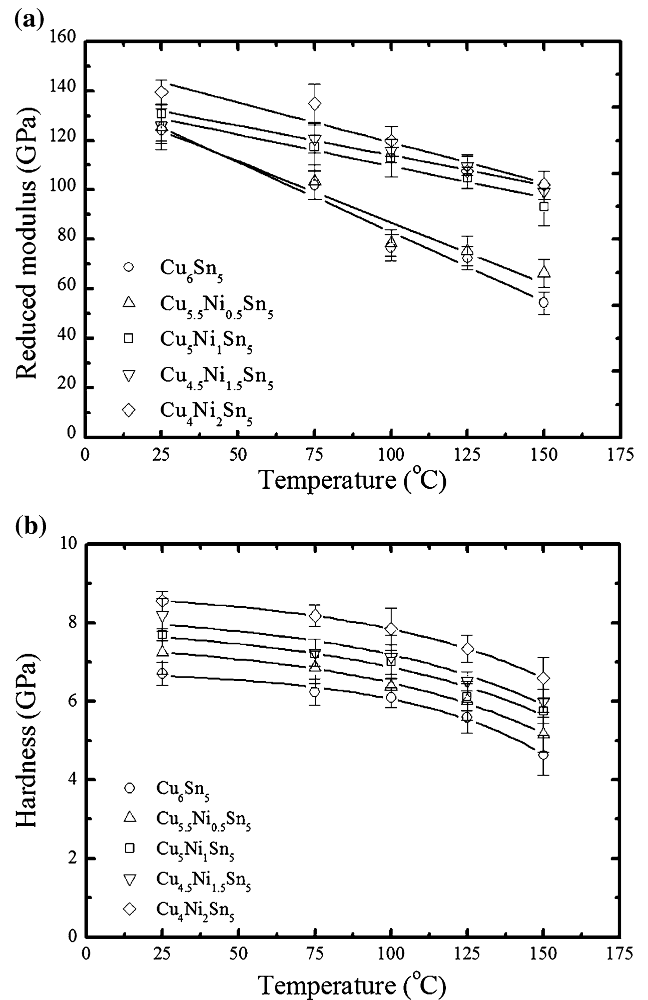

Fig. 2. (a) Reduced modulus of Cu_6Sn_5 and $(Cu,Ni)_6Sn_5$ at temperatures between 25°C and 150°C. (b) Hardness of Cu_6Sn_5 and $(Cu,Ni)_6Sn_5$ at temperatures between 25°C and 150°C.

i.e., $E \propto 1/(X_0)^N$.[31] As temperature was increased, the Cu_6Sn_5 expanded and the distance between atoms of Cu_6Sn_5 was elongated and the reduced

Table II. Parameters of fitting equations between reduced modulus and temperature of Cu_6Sn_5 and $(Cu,Ni)_6Sn_5$

Sample	E_{r25}	a	Reduced Modulus (GPa) Measured at 25°C
Cu_6Sn_5	125.29	0.56	124.3 ± 7.9
$Cu_{5.5}Ni_{0.5}Sn_5$	121.85	0.49	125.5 ± 6.6
$Cu_5Ni_1Sn_5$	131.24	0.20	126.3 ± 6.5
$Cu_{4.5}Ni_{1.5}Sn_5$	131.84	0.29	130.6 ± 4.3
$Cu_4Ni_2Sn_5$	143.46	0.33	139.5 ± 4.9

Table III. Parameters of fitting equations between hardness and temperature of Cu_6Sn_5 and $(Cu,Ni)_6Sn_5$

Sample	H_{25}	b	c	Hardness (GPa) Measured at 25°C
Cu_6Sn_5	6.75	−0.08	46.20	6.7 ± 0.7
$Cu_{5.5}Ni_{0.5}Sn_5$	7.52	−0.25	65.98	7.2 ± 0.6
$Cu_5Ni_1Sn_5$	7.91	−0.26	67.77	7.7 ± 0.2
$Cu_{4.5}Ni_{1.5}Sn_5$	8.21	−0.24	65.33	8.2 ± 0.4
$Cu_4Ni_2Sn_5$	8.77	−0.20	62.04	8.6 ± 0.3

modulus decreased. This explanation is supported by the increase of unit cell volume of Cu_6Sn_5 at elevated temperatures measured by synchrotron radiation. Moreover, Ni atoms could replace the Cu atoms in Cu_6Sn_5, resulting in substitutional defects associated with volumetric shrinkage. It has been found that Ni reduces the unit cell volume of Cu_6Sn_5 at temperatures between 30°C and 250°C,[23,24] which increases the reduced modulus of Cu_6Sn_5 as seen in Fig. 2a.

Using the nanoindentation results between 25°C and 150°C, an experimental linear relationship between the reduced modulus of $(Cu,Ni)_6Sn_5$ and temperature can be established as:

$$E_r = E_{r25} + a \cdot T, \tag{7}$$

where E_{r25} and a are constants calculated by linear regression. Table II summarizes E_{r25} and a values along with reduced modulus values for Cu_6Sn_5 and $(Cu,Ni)_6Sn_5$ measured at 25°C. The parameter a demonstrates the temperature dependence of the reduced modulus: a smaller a value indicates a faster decrease of the reduced modulus as the temperature increases. Figure 2b shows the hardness of $(Cu,Ni)_6Sn_5$ (x = 0, 0.5, 1, 1.5, 2) between 25°C and 150°C. It can be seen that the increase in temperature results in a significant decrease in hardness of Cu_6Sn_5, from 6.7 ± 0.69 GPa at 25°C to 4.63 ± 0.56 GPa at 150°C. This is reasonable because the melting point (onset of first liquid during heating) of Cu_6Sn_5 is 415°C[32] and the homologous temperature at 150°C is around $0.6T_m$. From the dislocation point of view, the decrease of hardness could be justified by the increased thermal vacancies of a material exponentially with temperature.[33] The generation of thermal vacancies at elevated temperatures therefore increased the dislocation activity and reduced the hardness of Cu_6Sn_5. The Ni was found to increase the hardness at temperatures from 25°C to 150°C. This is because of the Ni-induced substitutional defects that are likely to obstruct dislocation movement.

By regression fitting, the relationship between the hardness H of Cu_6Sn_5 and measurement temperature T was found to follow a decaying exponential equation:

$$H = H_{25} + b \cdot \mathrm{Exp}\left(\frac{T}{c}\right), \tag{8}$$

where H_{25}, b, and c are constants. Table III summarizes the values of H_{25}, b, and c along with hardness at room temperature for each chemical composition. The values of b and c indicate the effect of temperature on hardness: the smaller the values of b and c, the faster the decrease in hardness as the temperature increases.

The Arrhenius equation is often used to describe the decrease in hardness of lead-free solder alloys at elevated temperatures.[34] However, the decaying exponential relationship between hardness and temperature used in this study is different from the conventional Arrhenius equation. This is because the Arrhenius equation mainly represents the effect of increased thermal mobility during tensile testing. However, nanoindentation tests were performed using a sharp tip, which might create stress-induced vacancies due to the large deformation[35] and high stresses on the IMCs around the tip. These stress-induced vacancies affect the dislocation movement. As a result, the hardness and temperature of Cu_6Sn_5 and $(Cu,Ni)_6Sn_5$ have a different exponential relationship, rather than following the conventional Arrhenius equation.

Figure 3 shows the EDS spot analysis, BSE image of $Cu_{5.5}Ni_{0.5}Sn_5$, and distribution of Ni, Cu, and Sn elements in $Cu_{5.5}Ni_{0.5}Sn_5$. It can be seen that the

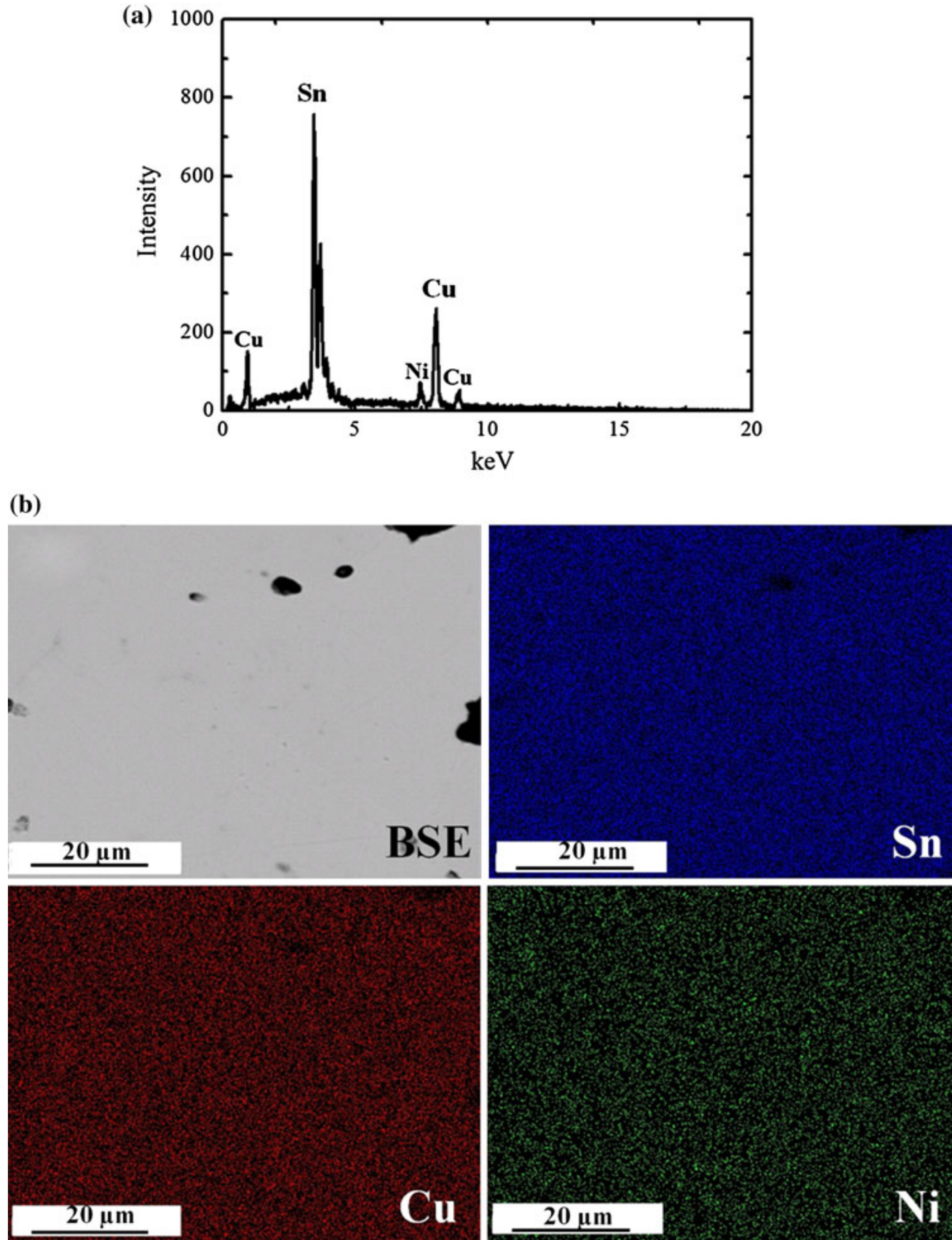

Fig. 3. (a) EDS spot analysis of $Cu_{5.5}Ni_{0.5}Sn_5$. (b) BSE image and distribution of Sn, Cu, and Ni in $Cu_{5.5}Ni_{0.5}Sn_5$.

sample has a homogeneous distribution of the major elements, with Ni evenly distributed in the $Cu_{5.5}Ni_{0.5}Sn_5$ sample as shown in Fig. 3b. Therefore, the effect of chemical segregation on the creep and mechanical properties is likely to be negligible.

Figure 4 shows representative creep displacements of Cu_6Sn_5 and $Cu_{5.5}Ni_{0.5}Sn_5$ at the peak load of 2000 μN as a function of dwell time at temperatures of 25°C, 125°C, and 150°C. Both primary and steady-state creep can be observed for Cu_6Sn_5 and $Cu_{5.5}Ni_{0.5}Sn_5$; rupture was not reached since relatively small peak loads and short dwell times were applied. At 25°C, the $Cu_{5.5}Ni_{0.5}Sn_5$ had less creep displacement than Cu_6Sn_5 during both primary and steady creep stages. At 125°C and 150°C, Cu_6Sn_5 had greater creep displacement during the primary stage, but the creep displacement of $Cu_{5.5}Ni_{0.5}Sn_5$ was greater than that of Cu_6Sn_5 during the steady stage. This time-dependent deformation behavior could affect the measurements of mechanical properties.

Using Eq. 5, the creep stress exponent was determined by log–log plotting of the creep strain rates and stresses, as shown in Fig. 5. At 25°C, the creep stress exponents of Cu_6Sn_5 and $Cu_{5.5}Ni_{0.5}Sn_5$ are 34.9 ± 2.7 and 43.1 ± 2.2, respectively. These results are in reasonable agreement with previous studies using nanoindentation.[15] As the temperature increased to 125°C and 150°C, the

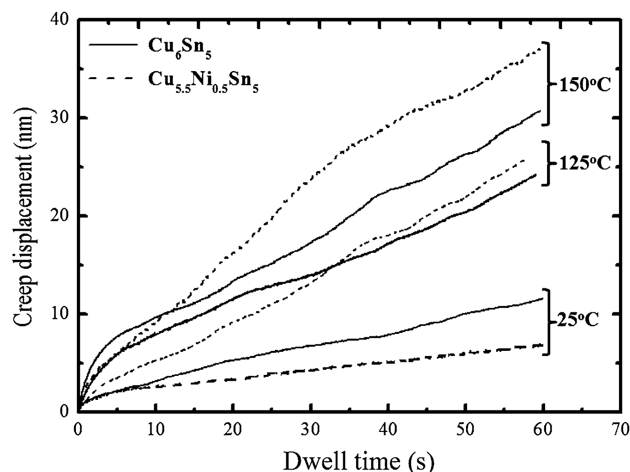

Fig. 4. Representative creep displacement of Cu_6Sn_5 and $Cu_{5.5}Ni_{0.5}Sn_5$ at 25°C, 125°C, and 150°C.

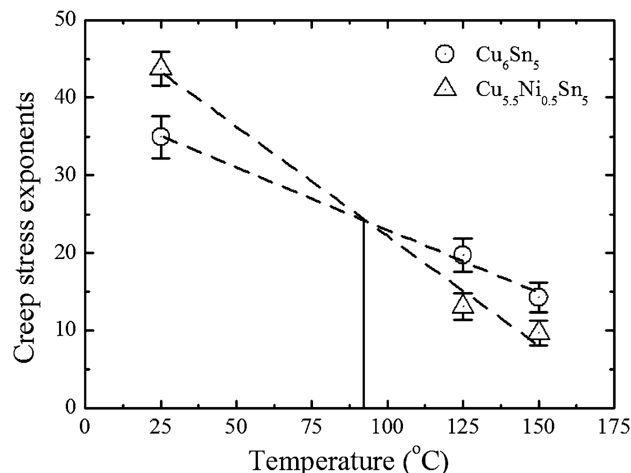

Fig. 6. Linear regression plotting of creep stress exponents of Cu_6Sn_5 and $Cu_{5.5}$ $Ni_{0.5}Sn_5$.

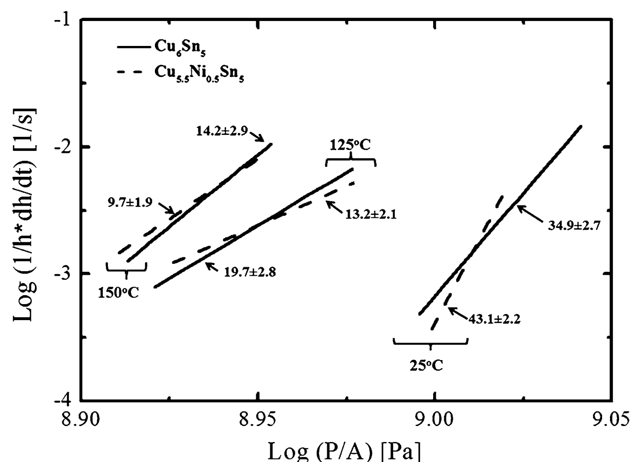

Fig. 5. Creep stress exponents of Cu_6Sn_5 and $Cu_{5.5}$ $Ni_{0.5}Sn_5$ at 25°C, 125°C, and 150°C.

creep stress exponents decreased to 19.7 ± 2.8 and 14.2 ± 2.9 for Cu_6Sn_5, and 13.2 ± 2.1 and 9.7 ± 1.9 for $Cu_{5.5}Ni_{0.5}Sn_5$, respectively, as shown in Fig. 5.

The decrease of creep stress exponent of Cu_6Sn_5 and $Cu_{5.5}Ni_{0.5}Sn_5$5 can contribute to the different creep mechanisms at 25°C and elevated temperature. At 25°C, the creep of Cu_6Sn_5 and $Cu_{5.5}Ni_{0.5}Sn_5$ is controlled by dislocation glide/climb and is independent of grain size when the creep stress exponent values are higher than 8.[26] However, at elevated temperatures, it is commonly known that the creep of a material is strongly dependent on the homologous temperature. At low homologous temperatures $<0.5T_m$, dislocation glide/climb controls the creep. At homologous temperatures $>0.5T_m$, either intergrain atomic diffusion or dislocation diffusion dominates the creep process depending on the applied stress and homologous temperatures.[30]

In this study, the creep of Cu_6Sn_5 and $Cu_{5.5}Ni_{0.5}Sn_5$ could be controlled by dislocation diffusion because of the high stress resulting from the sharpness of the indentation tip combined with the high homologous temperature: $0.58T_m$ at 125°C and $0.61T_m$ at 150°C. This statement is supported by the fact that the creep stress exponents of Cu_6Sn_5 and $Cu_{5.5}Ni_{0.5}Sn_5$ are higher than 8 (min. 9.7 ± 1.9 at 150°C), which suggests that the creep process is independent of the grain size and controlled by dislocation diffusion.[26] As the dislocation diffusivities of Cu_6Sn_5 and $Cu_{5.5}Ni_{0.5}Sn_5$ increase exponentially with temperature, the creep stress exponents of Cu_6Sn_5 and $Cu_{5.5}Ni_{0.5}Sn_5$ significantly decrease at elevated temperature, as shown in Fig. 5.

Assuming that the creep exponent decreased linearly with temperature, the variation of creep exponents of Cu_6Sn_5 and $Cu_{5.5}Ni_{0.5}Sn_5$ with temperature is plotted in Fig. 6. It can be found that the creep exponent of Cu_6Sn_5 exceeded that of $Cu_{5.5}Ni_{0.5}Sn_5$ for temperatures above approximately 90°C. Therefore, the Ni concentration showed variable effects on the creep behavior of Cu_6Sn_5: it impeded the creep of Cu_6Sn_5 at 25°C but increased the creep of Cu_6Sn_5 at elevated temperatures. From the Sn-Cu phase diagram,[32] the first liquid phase when heating Cu_6Sn_5 appears at 415°C and the homologous temperature of Cu_6Sn_5 at 90°C is around $0.53T_m$. Hence, it is reasonable to attribute the variable effects of Ni solubility on the creep of Cu_6Sn_5 to the difference in creep mechanisms at 25°C and elevated temperatures.

At 25°C, displacement glide/climb controls the creep process and the Ni-induced differences in bonding increase the creep stress exponent of Cu_6Sn_5 by obstructing dislocation movement. At elevated temperature, dislocation diffusion dominates the creep process and the addition of Ni reduces the creep stress exponents of Cu_6Sn_5 by stabilizing the hexagonal structure of Cu_6Sn_5 and

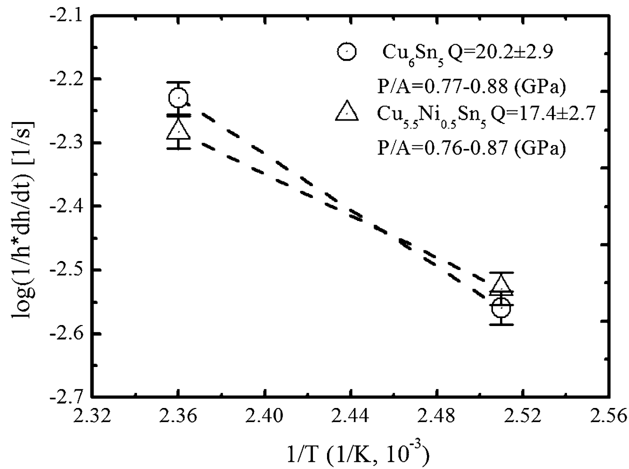

Fig. 7. Creep activation energies of Cu_6Sn_5 and $Cu_{5.5}$ $Ni_{0.5}Sn_5$ at 125°C and 150°C.

increasing the total energy of the hexagonal $Cu_{5.5}Ni_{0.5}Sn_5$ phase. This can be explained by comparing the total energy in monoclinic Cu_6Sn_5 and hexagonal $Cu_{5.5}Ni_{0.5}Sn_5$ phases obtained by first-principles calculation. It has been found that the monoclinic Cu_6Sn_5 phase has total energy (1.21 eV per two formula units at $T = 0$ K) lower than hexagonal Cu_6Sn_5 phase.[36] After addition of 5 at.% Ni, the total energy difference was reduced to be 0.90 eV per two formula units at $T = 0$ K, but the energetic order of monoclinic Cu_6Sn_5 and hexagonal $Cu_{5.5}Ni_{0.5}Sn_5$ remained the same.[36] This means that the total energy of hexagonal $Cu_{5.5}Ni_{0.5}Sn_5$ at 125°C or 150°C is higher than that of monoclinic Cu_6Sn_5.

According to our previous x-ray diffraction results[16] and time–temperature transformation (TTT) curve,[37] the Cu_6Sn_5 will transform into a monoclinic phase during the heat treatment for sample preparation. The presence of Ni, however, is associated with the formation of a metastable hexagonal phase, of higher total energy, as discussed above. This higher total energy of the metastable hexagonal $Cu_{5.5}Ni_{0.5}Sn_5$ is likely to have increased the atomic diffusion at elevated temperatures. As a result, the creep of $Cu_{5.5}Ni_{0.5}Sn_5$ is larger than that of Cu_6Sn_5 at elevated temperature.

By log plotting of the steady creep strain rates against the reciprocal of absolute temperature $1/T$ at a constant indentation stress $P_{\max}/A$, the creep activation energy of $Cu_{5.5}Ni_{0.5}Sn_5$ was calculated as 17.4 ± 2.7 kJ/mol at temperatures between 125°C and 150°C, which is smaller than the activation energy of 20.2 ± 2.9 kJ/mol for Cu_6Sn_5, as shown in Fig. 7. Therefore, the variable effects of Ni solubility on the creep of Cu_6Sn_5 can contribute to the Ni obstructing the dislocation movement at room temperature, but reduce the energy required to activate the dislocation diffusion in Cu_6Sn_5 at elevated temperatures.

CONCLUSIONS

The relationships between mechanical properties (reduced modulus and hardness) of $Cu_{6-x}Ni_xSn_5$ (x = 0, 0.5, 1, 1.5, 2) were elucidated at temperatures from 25°C to 150°C. Increase of temperature resulted in a decrease of the reduced modulus and hardness of Ni-free Cu_6Sn_5. The Ni solubility increased the reduced modulus and hardness of Cu_6Sn_5 between 25°C and 150°C. The creep stress exponents of Cu_6Sn_5 and $Cu_{5.5}Ni_{0.5}Sn_5$ were found to decrease as the temperature increased from 25°C to 150°C. The effect of Ni was to reduce the creep of Cu_6Sn_5 at 25°C, but increase the creep of Cu_6Sn_5 at 125°C and 150°C. It is proposed that the decrease of the creep stress exponents and the variable effects of Ni on the creep of Cu_6Sn_5 are due to different creep mechanisms at 25°C and elevated temperatures.

ACKNOWLEDGEMENTS

We gratefully acknowledge financial support from the University of Queensland–Nihon Superior Co. Ltd. collaborative research program and support from an Australian Research Council Linkage Grant LP100200250. The authors would like to thank Dr Y.Q. Wu and Mr. J. Read from the University of Queensland for their contributions to this research. D. Mu would like to acknowledge the financial support in the form of an Australian Postgraduate Award (APA).

REFERENCES

1. Y.C. Chan and D. Yang, *Prog. Mater. Sci.* 55, 428 (2010).
2. K.N. Tu, *Microelectron. Reliab.* 51, 517 (2011).
3. H.Y. Hsiao, C.M. Liu, H. Lin, T.C. Liu, C.L. Lu, Y.S. Huang, C. Chen, and K.N. Tu, *Science* 366, 1007 (2012).
4. J. Keller, D. Baither, U. Wilke, and G. Schmitz, *Acta Mater.* 59, 2731 (2011).
5. T. Laurila, V. Vuorinen, and J.K. Kivilahti, *Mater. Sci. Eng. R* 49, 1 (2005).
6. X. Deng, N. Chawla, K.K. Chawla, and M. Koopman, *Acta Mater.* 52, 4291 (2004).
7. L. Xu and J.H.L. Pang, *Thin Solid Films* 504, 362 (2006).
8. P.F. Yang, Y.S. Lai, S.R. Jian, J. Chen, and R.S. Chen, *Mater. Sci. Eng. A* 485, 305 (2008).
9. H. Tsukamoto, Z.G. Dong, H. Huang, and T. Nishimura, *Mater. Sci. Eng. B* 164, 44 (2009).
10. D. Mu, H. Tsukamoto, H. Huang, and K. Nogita, *Mater. Sci. Forum* 654, 2450 (2010).
11. N. Lee, V. Tan, and K. Lim, *App. Phys. Lett.* 88, 031913 (2006).
12. D. Mu, H. Huang, K. Nogita, *Mater. Lett.* 86, 46 (2012).
13. D. Mu, H. Yasuda, H. Huang, and K. Nogita, *J. Alloys Compd.* 536, 38 (2012).
14. M. Li, M. Yang, and J. Kim, *Mater. Lett.* 65, 1506 (2011).
15. J.M. Song, C.W. Su, Y.S. Lai, and Y.T. Chiu, *J. Mater. Res.* 25, 629 (2010).
16. K. Nogita, C. Gourlay, and T. Nishimura, *JOM* 61, 45 (2009).
17. K. Nogita, S.D. McDonald, H. Tsukamoto, J. Read, S. Suenaga, and T. Nishimura, *Trans. Jpn. Inst. Electron. Packag.* 2, 46 (2009).
18. T. Laurila, J. Hurtig, V. Vuorinen, and J.K. Kivilahti, *Microelectron. Reliab.* 49, 242 (2009).
19. F. Gao, T. Takemoto, and H. Nishikawa, *J. Electron. Mater.* 35, 2081 (2006).

20. C. Yu, J. Liu, H. Lu, P. Li, and J. Chen, *Intermetallics* 15, 1471 (2007).
21. K. Nogita and T. Nishimura, *Scrip. Mater.* 29, 191 (2008).
22. K. Nogita, *Intermetallics* 18, 145 (2010).
23. K. Nogita, D. Mu, S.D. McDonald, J. Read, and Y.Q. Wu, *Intermetallics* 26, 78 (2012).
24. D. Mu, J. Read, Y.F. Yang, and K. Nogita, *J. Mater. Res.* 26, 2660 (2011).
25. H. Huang, K.J. Winchester, A. Suvorova, B.R. Lawn, Y. Liu, X.Z. Hu, J.M. Dell, and L. Faraone, *Mater. Sci. Eng. A* 435, 453 (2006).
26. I.C. Choi, B.G. Yoo, Y.J. Kim, and J. Jang, *J. Mater. Res.* 1, 1 (2011).
27. Y.C. Liu, J.W.R. Teo, S.K. Tung, and K.H. Lam, *J Alloys Compd.* 448, 340 (2008).
28. Y.D. Han, H.Y. Jing, S.M.L. Nai, L.Y. Xu, C.M. Tan, and J. Wen, *J. Electron. Mater.* 39, 223 (2010).
29. F. Gao, H. Nishikawa, T. Takemoto, and J. Qu, *Microelectron. Reliab.* 49, 296 (2009).
30. R.W. Hertzberg, *Deformation and Fracture Mechanics of Engineering Materials*, 3rd ed. (New York: Wiley, 1989), p. 1.
31. H. Ma and J.C. Suhling, *J. Mater. Sci.* 44, 1141 (2009).
32. H. Okamoto, *Phase Diagrams of Dilute Binary Alloys* (Materials Park, OH: ASM International, 2002), p. 243.
33. D.R. Askeland, P.P. Fulay, and D. Bhattacharya, *Essentials of Materials Science and Engineering*, 2nd ed. (Stamford: Cengage Engineering, Stamford, 2009), p. 604.
34. Y. Sun, J. Liang, Z.H. Xu, G. Wang, and X. Li, *J. Mater. Sci.: Mater. Electron.* 19, 514 (2008).
35. W.C. Oliver and G.M. Pharr, *J. Mater. Res.* 7, 1564 (1992).
36. U. Schwingenschlögl, C. Di Paola, K. Nogita, and C. Gourlay, *Appl. Phys. Lett.* 96, 061908 (2006).
37. K. Nogita, C. Gourlay, S.D. McDonald, Y.Q. Wu, J. Read, and Q.F. Gu, *Scr. Mater.* 65, 922 (2011).